Rationalizing accurate structure prediction in the meta-GGA SCAN functional

Julia H. Yang, Daniil A. Kitchaev, and Gerbrand Ceder

Rationalizing accurate structure prediction in the meta-GGA SCAN functional

Julia Yang[1,2], Daniil Kitchaev[3], Gerbrand Ceder[1,2, *]

[1]Department of Materials Science and Engineering,

UC Berkeley, Berkeley, CA, 94720, USA

[2]Materials Science Division, LBNL, Berkeley, CA, 94720, USA

[3]Materials Department, UC Santa Barbara, Santa Barbara, CA, 93117, USA

*Correspondence and requests for materials should be addressed to G.C.

(email: gceder@berkeley.edu)

Abstract

The ability of first-principles computational methods to reproduce ground-state crystal structure selection is key to their application in the discovery of new materials, and yet presents a formidable challenge due to the low energy scale of the problem and lack of systematic error cancellation. The recently-developed Strongly Constrained and Appropriately Normed (SCAN) functional is notable for accurately calculating physical properties such as formation energies and in particular, correctly predicting ground state structures. Here, we attempt to rationalize the improved structure prediction accuracy in SCAN by investigating the relationship between preferred coordination environments, the description of attractive van der Waals (vdW) interactions, and the overall ground state prediction in bulk main group solids. We observe a systematic under-coordination error in the traditional Perdew, Burke, and Ernzerhof (PBE) functional which is not present in SCAN results and find that semi-empirical dispersion corrections in the form of PBE+D3 fail to correct this error in a consistent or physical manner. We conclude that the medium-range vdW interaction is correctly parameterized in SCAN and yields meaningful relative energies between coordination environments.

I. Introduction

Density functional theory (DFT) [1, 2] provides a robust approximation for the ground state energy and electron density of a many-body quantum system. It has been broadly useful in a variety of modern materials science challenges such as high-throughput predictions of properties of inorganic systems [3, 45, 46], rational design of energy storage materials [4], and in the generation of machine learning models for studying configurational entropy in multicomponent systems [47]. Answering these types of problems necessarily requires correct prediction of the ground state crystal structure as it profoundly influences nearly all material properties. However, completely reliable structure prediction remains elusive as the relative energies of competing structures tend to be small and affected by errors arising in various approximations to the exchange-correlation energy.

Approximations to the exchange-correlation energy are often categorized as "rungs of Jacob's Ladder of density functionals" [43]. The lowest rung refers to the local spin density approximation (LSDA) and assumes slowly varying electron densities. Despite being constructed to only strictly satisfy the homogenous electron gas limit, it has found reasonable success in a variety of solids [5-8], although it breaks down in molecular systems [9]. The next ladder rung introduces a dependence on the electron density gradient and is known as the generalized gradient approximation (GGA). One notable GGA is the Perdew, Burke, and Ernzerhof (PBE) functional [10], which has been generally successful in systems where LSDA is lacking [11, 12] and is often taken as a baseline functional for further case-specific corrections. These correction schemes address three major sources of error in PBE: a Hubbard U term to alleviate self-interaction error, interatomic potentials to introduce van der Waals (vdW) interactions, and fitted elemental corrections to compensate for incomplete error cancellation between condensed phases

and their elemental references. A third tier of functionals, referred to as meta-GGAs, introduces a dependence on the Kohn-Sham orbital kinetic energy density. A formal advantage of meta-GGAs is that they are able to recognize all types of orbital overlap, and thereby in principle simultaneously able to represent all types of chemical bonds [13]. The most successful meta-GGA to date is the Strongly Constrained and Appropriately Normed (SCAN) functional [14]. Compared to other non-empirical semi-local density functionals, SCAN has been shown to yield a significantly more accurate representation of the bulk properties of many semiconducting solids, including but not limited to formation enthalpy [24], bulk modulus, lattice parameter and volume [16], and reaction energies [17], transition pressures [39, 40]. However, while SCAN yields accurate properties for strongly-bound compounds [18] and ionic systems, it is moderately worse for weakly-bound intermetallic compounds [19] and significantly worse than PBE in overestimating of magnetic energies in metallic phases [15].

The practical impact of errors in functionals depends very much on what is being compared. An entirely discrete challenge for functionals is the ground state structure prediction problem because a ground state is either correctly stabilized or not. Only a limited number of case studies are available in the recent literature where SCAN is benchmarked on structure selection, focusing on MnO_2[20], FeS_2[21], Ce_2O_3, Mn_2O_3, Fe_3O_4[22], TiO_2 [23], as well as broad benchmarking work [24] on binary main group compounds observing that SCAN is more accurate than PBE in ground state structure prediction. However, there is no established rationalization of the origin of structure prediction accuracy given by the SCAN functional, except in systems where self-interaction is a known problem which can be addressed otherwise through a Hubbard U correction or higher order methods.

In this work, we purposely assess the structural errors in main-group closed-shell compounds arising from the PBE functional and explain the origin of accurate ground state prediction in SCAN. Of the three major sources of error in PBE – self-interaction, lack of vdW, and lack of error cancellation between condensed phases and elemental references – errors in structure selection may only be attributed to the first two factors. We isolate the effect of the vdW term by comparing results from pure PBE and SCAN to that given by a semi-empirical D3 vdW correction [52] in order to determine whether either of these conventionally-understood sources of error can explain the improvement in structure selection reliability reported for SCAN. We also include the SCAN+rVV10 functional [48] to determine if long-range corrections can improve structure selection accuracy in bulk ionic solids. We find that while vdW interactions significantly affect structure selection, a simple vdW correction to PBE yields unphysical trends in certain chemical spaces. Improvement in structure selection is thus only partially attributable to the presence of a vdW interaction and is highly dependent on the specific parametrization of this interaction. Instead, a consistent indicator of the proper representation of structural energies is the ability of the SCAN functional to choose experimentally-consistent coordination environments and unit cell volumes, leading us to speculate that proper parameterization of the exchange-correlation for crystal structure prediction must satisfy both criteria.

II. Methods

We base our analysis on 138 binary ionic compounds with formula A_xB_y, where cation A is {Li, Na, K, Rb, Cs, Be, Mg, Ca, Sr, Ba, B, Al, Ga, In, Tl, Si, Ge, Sn, Pb} and anion B is {N, P, As, Sb, Bi, O, S, Se, Te, F, Cl, Br, I}. Together, Table II and Table S1 list all the chemistries in this study, and they have also been presented by Zhang *et. al* [24]. Following this reference, we

consider experimental structures reported in the ICSD [25], as well as hypothetical structures derived via ionic substitutions onto likely crystal structures [26]. For example, for materials with chemical formula AB, the 11 candidate prototypes are listed in Figure S1.

The prototype of all relaxed structures is investigated using the StructureMatcher functionality in the pymatgen code [27] to detect where structures may have relaxed to other prototypes. In particular, we are interested in cases where input structures that were not set up as the experimental structure may have relaxed to the experimental ground state as this can generate false negatives, if not detected. Some of these are shown in Table S2b in [59]. The case where the experimental input structure relaxes to another type (possible false positive) is also detected. Statistics and examples are shown in [59]. The site distance threshold in StructureMatcher was set to $0.3v^{1/3}$ where v is the average volume per atom across the two structures. Average coordination numbers are calculated using the crystal nearest neighbor method in the pymatgen code [27], with details and validation given in [59].

We rely on the Vienna Ab-Initio Simulation Package (VASP) [28-29] for all calculations, using the same calculation parameters as reported by Zhang *et. al*. Specifically, we use Projector-Augmented Wave (PAW) potentials with a plane-wave cutoff of 520 eV and a reciprocal space discretization of 25 Å^{-1}. We converge all calculations to 10^{-6} eV in total energy and 0.01 eV A^{-1} in interatomic forces. The pseudopotentials used are listed in [59] in Table S3. We evaluate all structures with the PBE and SCAN functionals, as well as within the vdW-corrected PBE+D3 and SCAN+rVV10 functionals, and compare the performance of vdW-corrected PBE to the two variants of SCAN. Since the meta-GGA functional uses kinetic energy densities, a dense k-mesh may be required. We show in the Supplemental Information convergence with respect to the total number of irreducible k-points [59].

III. Results and Analysis

A. Dataset overview

We report the ground state structure mis-prediction rate for the four functionals, where a chemistry is considered incorrectly predicted by a functional if the energy of the experimental ground state structure is at least 1 meV/atom greater than that of a different structure as determined by the StructureMatcher algorithm. Table I lists these statistics for the 138 main group compounds.

Table I: Frequency of structure mis-prediction in PBE, PBE+D3, SCAN, SCAN+rVV10 for 138 main group compounds.

PBE	PBE+D3	SCAN	SCAN+rVV10
0.15	0.13	0.07	0.07

Table I shows that PBE has the highest mis-prediction rate among the four functionals, and that using the PBE+D3 functional adds a marginal improvement. SCAN reduces the error rate in PBE by half, while SCAN+rVV10 does not offer any improvement over SCAN.

The increased structure selection accuracy in SCAN can be best appreciated by inspecting the chemistries which are predicted incorrectly by at least one of the four functionals (Table II). Table S1 shows the rest of the chemistries that were correctly predicted by all four functionals.

We organize the mis-predicted cases by the anion group number from 15 (pnictide group) to 17 (halide group). Chemistries marked with an asterisk denote structures which have been synthesized experimentally in this chemistry but are not the ground state (e.g. they are known

metastable structures), and chemistries with no asterisk are structures which have never been

observed experimentally for that system.

Table II: Incorrectly predicted chemistries organized by anion group number. The positive value in parentheses is the absolute value of the energy (in meV/atom) of the DFT-predicted ground state structure relative to the experimental ground state structure. Asterisks denote ground states which are polymorphs that have been observed experimentally. A "–" indicates that the ground state is predicted correctly.

Group	PBE (meV/atom)	PBE+D3 (meV/atom)	SCAN (meV/atom)	SCAN+rVV10 (meV/atom)
15	–	NaP (7.55)	NaP (5.13)	NaP (6.73)
	–	Na_3Bi (3.88)	–	–
16	$GeSe$ (9.25)	$GeSe$ (2.36)	$GeSe$ (1.50)	$GeSe$ (8.79)
	TeO_2* (11.08)	TeO_2* (1.15)	–	–
	–	$GeSe_2$ (12.50)	–	$GeSe_2$* (8.73)
	SiO_2 (10.5)	–	–	–
	GeO_2* (2.04)	–	–	–
	SbO_2* (1.89)	–	–	–
	TeO_3 (21.61)	–	–	–
	–	$MgTe$* (49.98)	–	–
17	$CaBr_2$(20.58)	$CaBr_2$(13.20)	$CaBr_2$(6.69)	$CaBr_2$(5.46)
	SrI_2 (27.20)	SrI_2 (4.26)	SrI_2* (7.93)	SrI_2* (4.38)
	SnI_2 (33.86)	SnI_2 (9.18)	SnI_2 (12.98)	SnI_2 (5.12)
	$BiCl_3$ (53.35)	$BiCl_3$ (15.30)	$BiCl_3$ (6.41)	–
	–	$CaCl_2$* (2.25)	$CaCl_2$* (1.63)	$CaCl_2$* (3.17)
	SnF_2 (2.16)	SnF_2* (1.79)	–	–
	$TlCl$* (47.35)	$TlCl$* (43.08)	$TlCl$* (3.95)	–
	$LiCl$ (24.99)	$LiCl$ (1.65)	–	–
	$CsCl$* (47.87)	$CsCl$* (9.49)	–	–
	TlI* (23.20)	TlI (16.63)	–	–
	–	$LiBr$* (3.91)	–	$LiBr$ (9.53)
	LiF (4.70)	–	–	–
	$BaCl_2$* (24.02)	–	–	–
	$SnBr_2$ (3.05)	–	–	–
	$CsBr$* (40.13)	–	–	–
	$SrBr_2$ (13.74)	–	–	–
	$PbBr_2$* (29.22)	–	–	–
	CsI* (32.20)	–	–	–
	–	–	$TlBr$ (6.81)	–
	–	–	–	SnF_3 (13.83)

SCAN corrects several of the ground state errors of PBE, particularly in the halide

chemistries which will be discussed in the following sections. Furthermore, in several systems

where SCAN predicts an incorrect ground state (e.g. GeSe, CaBr$_2$, SrI$_2$), it moves the error in the

correct direction with respect to PBE. Still, a few errors are increased by SCAN over PBE (NaP, $CaCl_2$, TlBr). We discuss a few cases from Table II in more detail below.

i. SrI₂

Table II shows that the ground state structure for SrI_2 in all functionals is incorrect. The experimental ground state (space group *Pbca*, seven-fold coordination) has two iodine sites, described as having one I coordinated to Sr in a trigonal plane and the other coordinated to Sr tetrahedrally [69].

The ground state in PBE is a layered structure (space group *P-3m1*) which has never been observed experimentally for this chemistry. Likewise, PBE+D3 predicts a ground state (space group *P-1*) which also has never been seen experimentally. In contrast, the ground state in SCAN and SCAN+rVV10 is the metastable SrI_2 structure (space group *Pnma*) which is synthesized via slow dehydration of its monohydrate form, $SrI_2 \cdot H_2O$ [34]. This polymorph contains tetrahedral I-Sr and distorted trigonal planar I-Sr environments and the tetrahedral I-Sr symmetry is captured well in SCAN and SCAN+rVV10, unlike in PBE+D3 which distorts the I-Sr tetrahedral bonds resulting in a lower symmetry structure. In summary, while no ground states are correctly predicted in any of the functionals, SCAN and SCAN+rVV10 notably predict a successfully-synthesized polymorph.

ii. CaCl₂

The ground state of $CaCl_2$ is orthorhombic (space group *Pnnm*), but it is known that $CaCl_2$ crystals undergo a second-order ferroelastic transition to the α-PbO_2 phase at high temperature [35]. The two phases have the same local coordination and only differ in volume by 1%. All functionals except PBE over-stabilize this higher-pressure phase by a few

9

meV/atom, and the dispersion-corrected functionals worsen the accuracy by exacerbating the over-stabilization of a higher pressure polymorph.

We also note the geometric features of orthorhombic $CaCl_2$ as calculated within each functional. Table III and Figure 1 describe the two different Ca-Cl distances in the $CaCl_6$ octahedron and the lattice parameters, showing how the Ca-Cl bond lengths in SCAN are closest to experimental values [37]. Furthermore, in every feature, SCAN never stabilizes a value that is furthest away from the experimental value because it never makes the largest error which are colored in red. Meanwhile, PBE makes the largest errors in the Ca-Cl bond lengths, PBE+D3 and SCAN+rVV10 have the largest error in *a* lattice parameter, PBE has the largest error in *b* lattice parameter, and PBE+D3 over-binds the most in the *c* lattice parameter. This finding that SCAN improves lattice parameters over PBE is consistent with previous studies [16, 38], and we additionally observe that despite the lack of the correct ground state for $CaCl_2$, the structural features of the experimental ground state in SCAN are more accurate than in PBE which is the only functional to stabilize the experimental ground state.

Table III: Structural features of the orthorhombic $CaCl_2$-structure ground state as determined experimentally [37] and calculated by PBE, PBE+D3, SCAN, and SCAN+rVV10. The Ca-Cl bond length and lattice constants and percent deviation from experiment are shown in the structure to the right generated by VESTA [73], with the largest deviations from experiment per geometric feature highlighted in red.

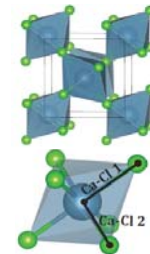|	Exp.		PBE		PBE+D3		SCAN		SCAN+rVV10	
	(Å)	%	(Å)	%	(Å)	%	(Å)	%	(Å)	%
Ca-Cl 1	2.74	–	2.78	1.46	2.73	-0.22	2.74	0	2.73	-0.36
Ca-Cl 2	2.74	–	2.76	0.73	2.73	-0.21	2.74	0	2.73	-0.36
a	4.18	–	4.19	0.24	4.14	-0.96	4.16	-0.48	4.14	-0.96
b	6.44	–	6.55	1.71	6.48	0.62	6.47	0.47	6.45	0.16
c	6.29	–	6.32	0.48	6.14	-2.38	6.27	-0.32	6.25	-0.64

Figure 1

iii. SnI$_2$

While the ground state in SnI$_2$ is incorrectly predicted across all functionals, the magnitude of error is lowest for PBE+D3 and SCAN+rVV10, followed by SCAN then PBE. All four functionals stabilize a layered structure (space group *P-3m1*) with octahedral symmetry instead of the monoclinic structure (space group C2/*m*). Howie *et. al* [68] described the structure to contain two distinct metal sites, where two-thirds of the Sn atoms occupy environments similar to that of Pb in the PbCl$_2$ structure (i.e. a trigonal prism with an additional bond for a total coordination of seven). The last third of Sn sit in an octahedron where four of the I atoms form PdCl$_2$-type chains and the other two I are slightly further away (~0.02 Å). The PdCl$_2$-type environment is interlocked with the PbCl$_2$-type environment. Howie *et. al* summarized that the structure is layered in a dual sense: First, that the I belonging to both PdCl$_2$-type and PbCl$_2$-type environments form tightly puckered (201) sheets loosely connected by long Sn-I bonds, and second, that crystallographically the structure shows (010) layering. The authors were not able to use Mössbauer spectroscopy on the Sn quadrupoles to resolve the two distinct Sn sites due to a lower-than-expected isomer shift, and concluded that one of the Sn in the unit cell could not be purely ionic. Howie *et. al* suggested that if some *5s* electrons are involved in the conduction bands, the Mössbauer spectrum could be better explained. Clearly, the SnI$_2$ structure remains to be completely resolved both experimentally and via first-principles methods. While it is possible that a hybrid functional may be able to correctly predict the ground state of SnI$_2$, we find here that SCAN+rVV10 captures the energy of the layered ground state structure most consistently with experiment. (An extended discussion on ground state prediction of layered materials will follow.)

iv. TlBr

The ground state for TlBr is the CsCl structure [70] and correctly predicted by all
functionals, except in SCAN, which stabilizes the orthorhombic structure (space group *Cmcm*), a
prototype which has never been observed experimentally for this chemistry. In fact, this *Cmcm*
structure is actually the ground state for TlI, although it can be observed in ternary Tl-Br-I
phases, $TlBr_{1-x}I_x$, where x > 0.3 [71]. The ground state of TlI contains seven-fold coordinated
environments, where five of the bonds are coordinated in a rectangular pyramid (one bond is
3.36 Å and the other four are 3.49 Å) and the last two bonds are longer, at 3.83 Å. Samara *et. al.*
[72] described this structure to be a compromise between NaCl-type and CsCl-type structures
given that both prototypes are ground states for other Tl-halides and that the local coordination
of *Cmcm* takes on an intermediate value of seven. The authors reasoned that the TlI ground state
is stabilized through the polarizability of the Tl ion and the tendency for I to make covalent
bonds. Based on the structural analysis on TlI by Samara *et. al*, we hypothesize that the SCAN
functional may predict more covalent Tl-Br bonds than what is observed experimentally,
resulting in an incorrect ground state. Given the small energy differences involved, it is possible
that spin-orbit interactions, not included in this work, would modify the structural energetics for
these heavy elements.

Only a few cases from Table II have been discussed but they reveal several trends:
Sometimes, the predicted ground state has never been observed experimentally in that system,
implying that it is not even a metastable phase. This is the case for the SrI_2 structure predicted by
PBE and PBE+D3, the layered SnI_2 predicted by all four functionals, and the polymorph of TlBr
predicted by SCAN; Other times, functionals stabilize the higher-pressure polymorph, such as

PBE+D3, SCAN, and SCAN+rVV10 for $CaCl_2$. We note that adding dispersion corrections further bind the anions in $CaCl_2$ and exacerbates the stabilization of lower volume polymorphs.

v. General comments

While Table I summarizes that structure selection is on average most accurate in the SCAN functional, Table II alternatively details how certain chemistries are mis-predicted by SCAN but correctly predicted by another functional (in parentheses): NaP (PBE), TlBr (PBE, PBE+D3, SCAN+rVV10), $CaCl_2$ (PBE). Unfortunately, it does not seem possible a-priori to state which functional will get the ground state correct, when SCAN does not.

Table II also elucidates why the PBE+D3 functional does not approach the same structure prediction accuracy despite including dispersion interactions. While some chemistries are corrected by both PBE+D3 and SCAN (e.g. LiF, $BaCl_2$, $SnBr_2$), a number of other chemistries are predicted correctly in SCAN and not in PBE+D3 (e.g. TeO_2, SnF_2, LiCl). Furthermore, there are even chemistries which are correctly predicted in PBE but not in PBE+D3: Na_3Bi, $GeSe_2$, MgTe, $CaCl_2$, LiBr. Surprisingly, the MgTe ground state is incorrectly predicted to be rocksalt in PBE+D3 by around 50 meV/atom below the true ground state. A discussion on this outlier and rationale for why certain chemistries are mis-predicted in PBE+D3 but correctly predicted in PBE is given in section C.

B. Structural trends

A trend emerges when all ground states stabilized by each functional are analyzed. Figure 2 shows the average cation-anion coordination in the predicted ground state relative to the average cation-anion coordination in the experimental ground state plotted with the over-stabilization energy, which is the energy difference between the DFT ground state and the experimental ground state. By definition this energy is negative. The blue and red regions show when the DFT

ground state has a lower or higher coordination than the experimental ground state, respectively.

For example, in SrI_2, where the PBE predicted ground state has a six-fold cation-anion

coordination and the experimental structure has a seven-fold cation-anion coordination, the

coordination difference predicted by PBE is -1.
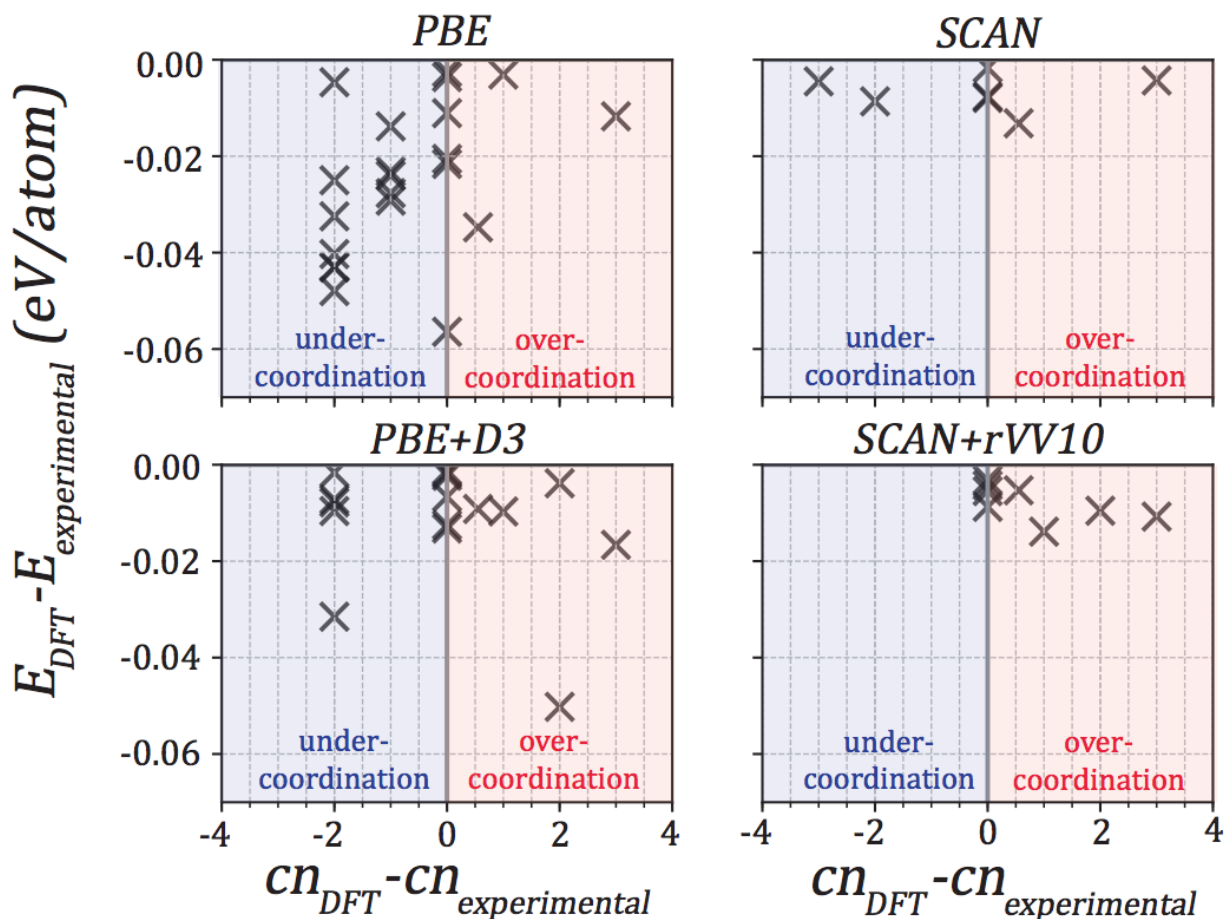
Figure 2: Cation-anion coordination environments of all incorrectly predicted ground state chemistries for the four functionals. The x-axis is the average coordination number (*cn*) of the DFT ground state structure relative to that of the experimental ground state structure. The y-axis is the DFT over-stabilization energy (meV/atom). A negative relative coordination indicates that the functional stabilizes a structure with lower coordination. A positive value means the functional stabilizes a higher coordination.

Figure 2 indicates that PBE tends to under-coordinate the cation because many of the PBE

ground states have lower relative coordination than the experimental ground state. A number of

14

systems are under-coordinated by at least two bonds in PBE. In fact, this preference for PBE to favor under-coordination is noticeable even when the correct ground state is obtained. Figure 3 shows the relative energies between higher coordinated (rocksalt) and lower coordinated (zinc blende) structures in the Na-halide, K-halide, Ca-chalcogenide, Sr-chalcogenide, and Ba-chalcogenide systems. For all these systems, the experimental ground state is rocksalt. While for the Na, Ca, K, and Sr chemistries in Figure 3, PBE correctly predicts rocksalt as the ground state, it consistently determines the rocksalt energy advantage to be smaller by tens of meV/atom relative to the other functionals. In the Cs-halides, the PBE error is more dramatic. Here, the energy of the CsCl-type structure (the ground state for CsCl, CsBr, and CsI) is compared to that of the rocksalt structure, which is the ground state for CsF. In this case the preference for under-coordination causes PBE to mis-predict the stable structure for all the bigger halogens.

Figure 3 demonstrates that functionals agreeing on the ground state structure may still represent relative polymorph stabilities differently. Accurate differences between polymorphs are critical in challenges such as synthesis of metastable compounds [62].

While it would be useful to contextualize these polymorph energies with experimental data, we were not able to find experimental values for polymorph energy differences in alkali halide and alkali-earth chalcogenide structures. Blackman et. al [70] give qualitative descriptions of potentially existing polymorphs in CsCl, CsBr, and CsI. Thin films of CsBr and CsI deposited on amorphous substrates at low temperatures showed weak diffraction rings corresponding to the rocksalt structure coexisting with stronger diffraction rings from the cesium-chloride structure. These rock-salt pattern disappeared well before room temperature. However, no calorimetry measurements were performed, so no polymorph energies were given.
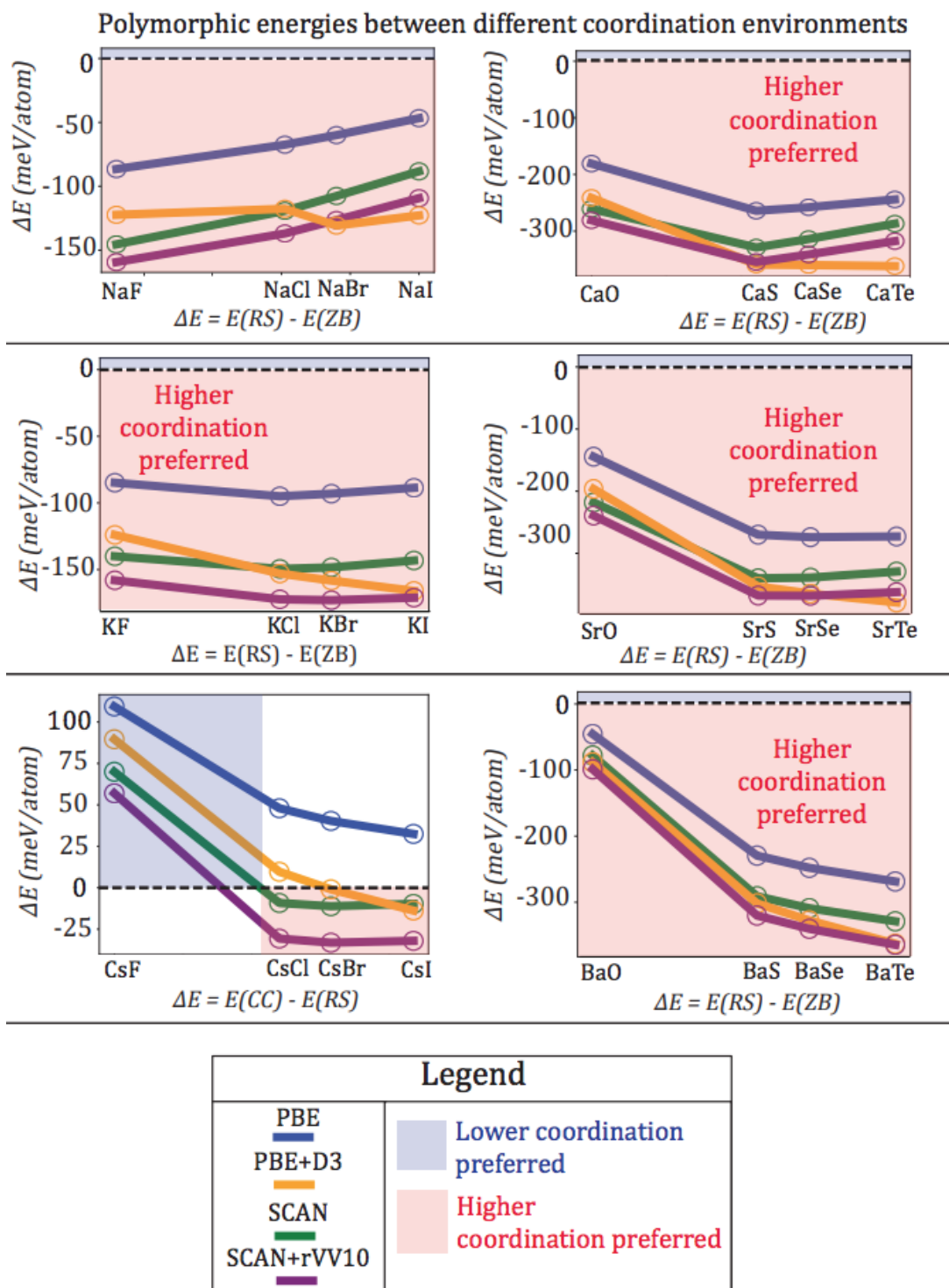
Figure 3: Energy differences of high and low coordination polymorphs for various alkali-halide and alkaline-earth chalcogenides ordered by anion size. The listed structures are rocksalt (RS), wurtzite (WZ), zinc blende (ZB), cesium chloride (CC). Regions in red indicate the ground state is the higher coordinated structure while regions in blue indicate the opposite.

With the dispersion correction, PBE+D3 no longer has systematic under-coordination because fewer ground state structures have negative relative coordination as seen in Figure 2. In fact, polymorph energies in Figure 3 show that higher coordination is more preferred in PBE+D3 compared to in PBE since the rocksalt - zinc-blende polymorph energies are shifted down in energy by at least 40 meV/atom. This bias is especially strong in the K-halides, Cs-halides, Ca-chalcogenides, Sr-chalcogenides, and Ba-chalcogenides.

In contrast, no systematic error in coordination preference is observed in SCAN in either ground state environments in Figure 2 or in the polymorph energies in Figure 3. Since volume and lattice parameters derived in SCAN are found to be closest to experimental values [16, 38] and do not have systematic over-binding or under-binding, we suppose that the densities, and therefore the coordination environments in SCAN should also be reasonable.

C. Non-physical errors in PBE+D3

We examine MgTe, over-predicted in PBE+D3 by 50 meV/atom, and the last set of alkali-halides which have yet to be discussed: LiF, LiCl, LiBr, and LiI. While most alkali-containing binary compounds are rocksalt structures, as evidenced in Figure 3, the ground states for LiBr, LiI, and MgTe are wurtzite.

This preference for lower-coordination in LiBr, LiI, and MgTe can be understood by considering the anion-anion distance in structures. The anion-anion distance in a higher coordinated polymorph is less than the anion-anion distance in a lower coordinated polymorph, as evidenced by Figure S4 for all alkali-halide and alkali-earth-chalcogenide compounds. (For example, in LiI the anion-anion distance in rocksalt is 4.247 Å, which is smaller than the anion-anion distance in wurtzite which is 4.513 Å.) Therefore, with increasing anion radius, structures

with larger anion-anion separation should be energetically favored according to Pauling's radius ratio rule [41], so we expect a stronger preference for lower coordination.

We assess whether the functionals capture this fundamental trend. Figure 4 shows the polymorphic energy difference between higher and lower coordinated structures for the Li-halide and Mg-chalcogenide families as a function of the anion size. The shaded blue or red areas define where a functional stabilizes a structure with lower or higher coordination than the ground state, respectively. For example, since the PBE predicted ground state for LiCl is wurtzite which is incorrectly positioned 24.95 meV/atom below the true rocksalt ground state, the point for PBE falls in the blue region labelled "under-coordinated ground state."
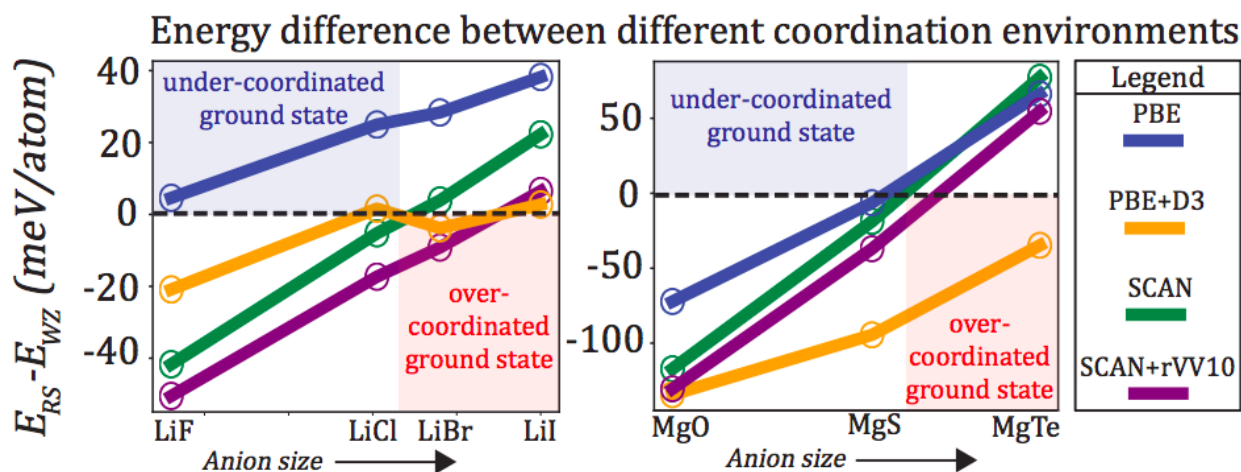
Figure 4: Energy difference between rocksalt and wurtzite structures for the Li-halide and Mg-chalcogenide chemistries with the four functionals. The colored regions in blue or red emphasize when the ground state is incorrectly predicted to be wurtzite or rocksalt, respectively.

From Figure 4, we observe that as the anion radius increases from F to Cl in the Li-halides, the relative stability of the rocksalt structure with respect to wurtzite decreases as expected.

Even PBE which gets the ground states of LiF and LiCl incorrect does capture the trend that with increasing anion size, lower coordination environments should become more stable.

Remarkably, the slope of the rocksalt-wurtzite energy difference with anion size is similar for

PBE, SCAN, and SCAN+rVV10. Hence, while PBE captures this trend properly, its incorrect prediction of LiCl and LiF seems to stem from an absolute bias towards lower coordination.

In contrast, we observe that PBE+D3 fails to capture the energy dependence on anion size for the Li-halides because the slope does not follow the monotonic increase observed in the other three functionals. PBE+D3 in fact demonstrates a systematic preference for higher-coordinated structures since the decreasing stability of the higher-coordinated polymorph with anion size is either absent (K-halide, Cs-halide, Ca-chalcogenide, Sr-chalcogenide, Ba-chalcogenide) or largely reduced (Li-halide, Na-halide, Mg-chalcogenide) compared to that in other functionals. Hence, while the semi-empirical PBE+D3 dispersion appears to reduce the error in PBE by correcting the ground state in LiF and reducing the over-stabilization error in LiCl, it confounds polymorphic stabilities and fails to capture fairly basic crystal chemical trends.

A. Comments on SCAN+rVV10

We find in this study on bulk solids that the long-range vdW contribution in SCAN+rVV10 is dictated, to first order, by coordination (*cn*) and not by chemistry, meaning that

$$E_{SCAN+rVV10}(AB, BB, cn) \sim E_{SCAN}(AB, BB, cn) + vdW^{long-range}(cn)$$

where AB indicates cation-anion bonds and BB indicates non-bonding anion-anion interactions. Since the SCAN+rVV10 polymorph differences in Figure 3 and Figure 4 are roughly a constant shift from the SCAN polymorph energies, then it appears that different anion chemistries in the same framework do not contribute additional long-range vdW interactions.

However, this observation may not be true for vdW solids given that dispersion interactions account for a greater fraction of the total cohesive energy in this class of structures. We therefore tested SCAN+rVV10 in Cs$_2$O (space group *R-3m*), a layered material, and compare the results

with the other functions. We calculate the energy of the experimentally-determined structure (a = b = 4.256 Å, c = 18.99 Å, $\alpha = \beta = 90°$, $\gamma = 120°$) [63] and of structures for which the c-lattice parameter is compressed or expanded. All ions are allowed to fully relax inside a fixed volume cell. Figure 5 shows the predicted *c* lattice parameters, indicating how SCAN+rVV10 most closely agrees with experiment. PBE over-estimates *c* and predicts the lowest bulk modulus which is a known problem in PBE [64]. PBE+D3 and SCAN over-predict the slab spacing by 0.7 Å and 0.4 Å, respectively.
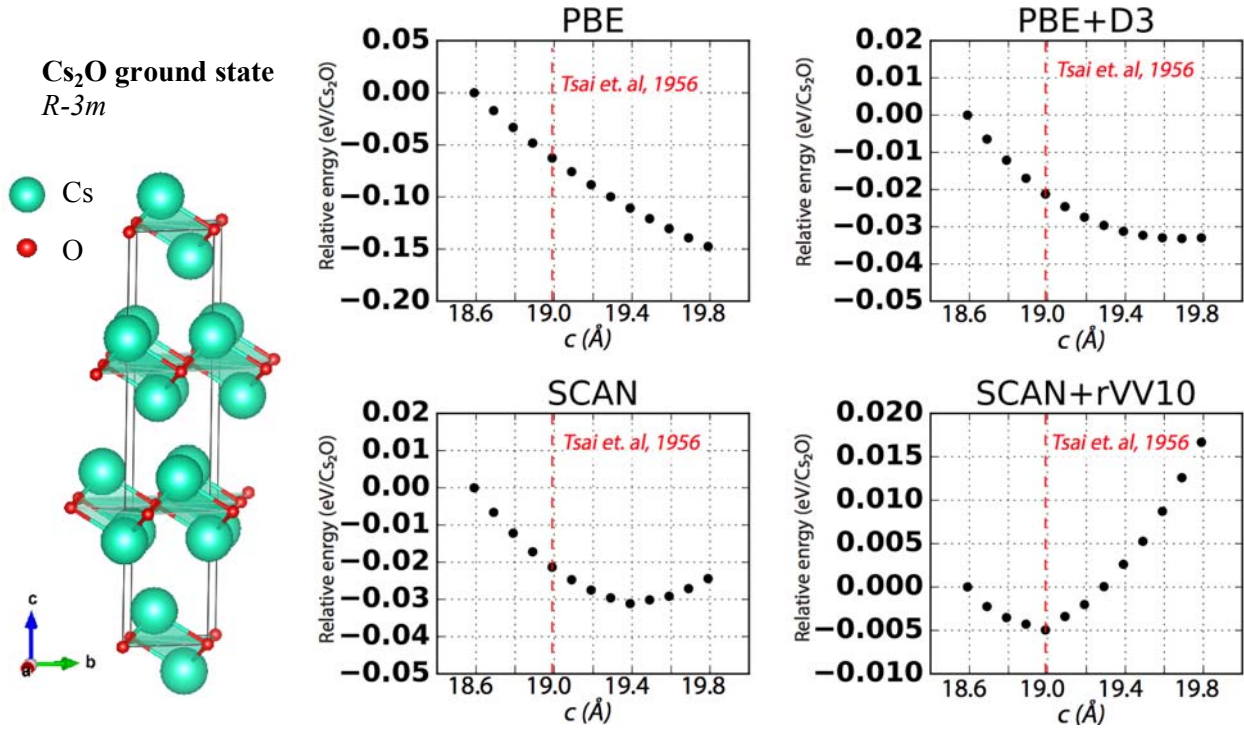
Figure 5: Cs_2O ground state structure predicted stability of varying *c* lattice parameter. The experimentally-determined value by Tsai *et. al* [63] is indicated by the red dashed line.

It is not all that unexpected that the predictions in SCAN+rVV10 for a layered material are closest to experimental values. In a set of 11 representative vdW structures benchmarked with 11 vdW methods, Tawfik *et al* [53] found that SCAN+rVV10 gives the lowest mean average error for binding energy and *c* lattice spacing and suggested that functionals which include damping functions connecting the dispersion correction to the underlying exchange-

correlation functional simply cannot meet the competing demands of both correct energies and correct geometries. In our study, PBE+D3 is such a case in point when compared to SCAN+rVV10. Additionally, Peng *et. al.* [48] benchmarked interlayer spacings and intralayer lattice constants in 28 layered materials which found that SCAN+rVV10 can reproduce interlayer spacing more accurately than SCAN due to the consideration of longer-range vdW in an effective range of 8-16 Å. Therefore, the advantage of SCAN+rVV10 over SCAN appears to manifest itself in vdW solids.

IV. Discussion

From our detailed study of ground state prediction in binary ionic compounds where self-interaction is not as prominent as in transition metal systems, we find that the prediction of ground state structures in SCAN is on average more accurate than in PBE, PBE+D3, or SCAN+rVV10 (Table 1). Furthermore, SCAN does not improperly favor certain metal-anion coordination environments because it neither under-coordinates nor over-coordinates (Figure 2). In the $CaCl_2$ case study in Figure 1 and Table III, SCAN most accurately predicts geometric features of the experimental ground state despite under-stabilizing the structure, even more so than the PBE functional despite it being the only functional to correctly stabilize the ground state.

The reliability of the SCAN functional in predicting ground state structures is related to its reliability in choosing local environments (i.e. coordination number, connectivity) consistent with experiment. We surmise that a signature of the capability of an exchange-correlation functional to predict crystal structure is a lack of systematic error in coordination number and lattice volume.

It has been argued [14, 48] that because the exchange enhancement factor in PBE,

$F_x(s) = 1 + \kappa - \frac{\kappa}{1+\mu s^2}$, where $s = |\nabla n|/(2(3\pi^2)^{\frac{1}{3}}n^{\frac{4}{3}})$, approaches the Lieb-Oxford bound of

1.804 for large density gradients s, molecules can lower their energy by moving further apart.

We recapitulate this argument in Figure 6 by plotting the exchange enhancement factor F_x for

PBE [10] and SCAN [14] for the different types of bonding relevant to this study: covalent

($\alpha = 0$) and ionic ($0 < \alpha < 1$). Since the exchange energy $E_x[n] = \int d^3rn\epsilon_x^{unif}(n)F_x(s)$ is

negative by construction ($\epsilon_x^{unif}(n) = -(\pi)(3\pi^2n)^{\frac{1}{3}}$ and $F_x(s)$ is monotonic and positive), larger

density gradients s always yield a more negative exchange energy. By construction, this form of

the exchange artificially lowers the energies in all structures which have maximal electron

gradients or minimal electron-electron overlap.

Our study of structure selection focuses on systems with closed-shell anions for which

electron density is high on the anion, suggesting that the anion-anion distance, or the extent to

which electron densities are non-overlapping, is the key descriptor for identifying differences

among how the functionals evaluate energies. PBE consistently favors minimal electron density

overlap, resulting in two possible scenarios: the first is to increase the distance between metal-

anion centers, and the second is to include fewer anions in the first anion shell. In fact, both

outcomes are observed in our study: (1) the bond lengths in $CaCl_2$ as calculated by PBE are

always over-predicted (Table III), a known general problem in PBE [49, 50]; and (2) there is

systematic preference to include fewer anions in the first anion shell, resulting in lower

coordination (Figure 2). We conclude that the analytical form of exchange enhancement factor in

PBE artificially shifts structures with those characteristics (large lattice parameters, lower metal-

anion coordination) to a lower energy, explaining the high error rate in structure selection

accuracy in the PBE functional.
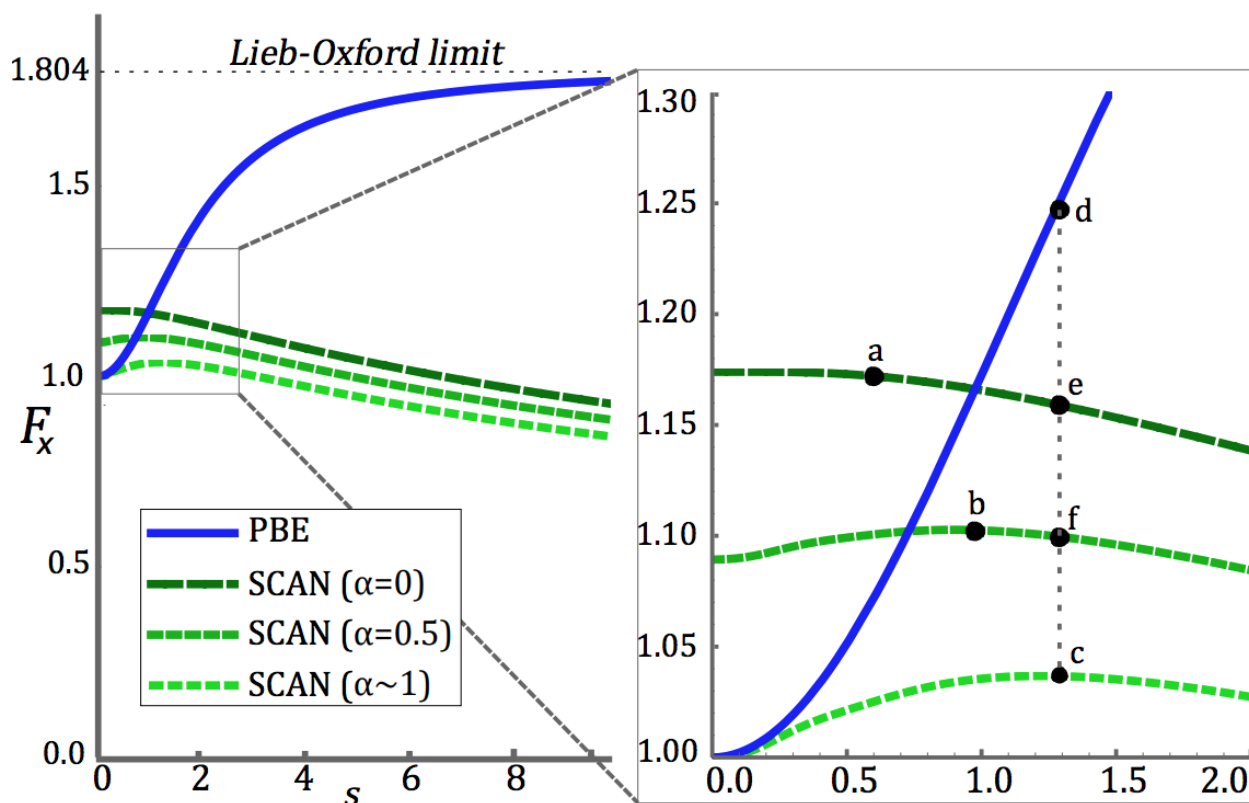
Figure 6: The exchange enhancement factor, F_x, for PBE and SCAN for various types of bonding ($\alpha = 0, 0.5, \sim1$) for large (left) and small (right, figure inset) gradient s. The points a, b, c indicate inflection points in F_x and c, e and f mark different F_x for the same gradient s.

In contrast, the exchange enhancement factor in SCAN, $F_x(s, \alpha)$, does not approach the Lieb-Oxford bound [44, 51] for any type of bond or α value, and also can either favor or disfavor density-density interactions because F_x contains an inflection point (e.g. points a, b, and c in Figure 6). The vdW interactions are "activated" at the inflection point, which first prevents the exchange enhancement factor from increasing without bound and second favors density-density interactions, two features crucially missing in PBE. Interestingly, for decreasing bond strength (increasing), the inflection point occurs at larger density gradient s, indicating that these intermediate-range vdW interactions in SCAN are sensitive to different types of bonding.

The inset in Figure 6 also shows how different types of bonding generate greater differences in exchange enhancement factors. For example, $F_x(s)^{PBE} - F_x(s, 0.5)^{SCAN} > F_x(s)^{PBE} - F_x(s, 0)^{SCAN}$, e.g. the difference between points d and f is larger than the difference between d and e. We hypothesize that structure selection problems involving weakly-bound solids where vdW interactions form a greater fraction of the cohesive energy may uncover even greater differences between PBE and SCAN.

We conclude that the origin of the increased accuracy in SCAN in ionic main group compounds is the inclusion of appropriately-parameterized medium-ranged vdW interaction between anions. Since the vdW interaction is attractive, SCAN correctly stabilizes the smaller anion-anion distances in select scenarios, leading to the stabilization of higher-coordinated structures where PBE fails. Thus, the vdW interaction not included in the PBE functional can be reliably accounted for in the SCAN functional.

The semi-empirical PBE+D3 correction changes the systematic errors in PBE discussed earlier but does not systematically reduce the structure mis-prediction error because chemistries which are correctly predicted in PBE are sometimes mis-predicted in PBE+D3 (Table II). We reason this anomaly arises from the attractive dispersion on the anions which lowers the energy of structures with shorter anion-anion distances with respect to structures with longer anion-anion distances, a circumstance of the analytical form of the D3 correction. Since anion-anion distances in higher-coordinated structures are consistently shorter than anion-anion distances in lower-coordinated structures (indicated in Figure S4), PBE+D3 consistently stabilizes higher-coordinated structures.

While for certain cases this correction results in reduced error, such as in LiF and LiCl, in other cases it also leads to mis-prediction, such as LiBr. The consistent stabilization of higher-

24

coordinated structures violates Pauling's radius ratio rule and fails to reproduce the original polymorph stabilization orderings in PBE (Figures 3 and 4). Evidently, the D3 correction on average somewhat improves ground state prediction, but misses classic stability rules.

We speculate that it may be challenging for the semi-empirical D3 correction to accurately parameterize the anion-anion interactions based only on the atomic structure and not the electronic (density) structure which is the method by which SCAN and SCAN+rVV10 include the attractive vdW interactions. In the latter, the long-range vdW correction includes strictly pairwise interactions between volumes of electron densities and maintains a consistent description of polymorphic stabilities across chemical systems because it only contributes a constant energy shift in Figures 3 and 4.

We conclude that *ab initio* studies of the relative stability of structures necessarily require consideration of vdW forces treated at an electronic density level, as is done in the meta-GGA SCAN functional, as these interactions are critical to structure selection and empirical forms of vdW attraction based on atomic configuration alone confound physical trends in structure stability.

In this study we purposefully excluded transition metals and rare earth containing-compounds to separate the self-interaction error from the lack of dispersion in PBE. In fact, several structure selection studies have pointed out the persistence of the self-interaction error in the SCAN functional because enforcing a Hubbard U value is necessary to obtain the correct ground state in TiO_2 [23], Ce_2O_3, Fe_3O_4, α-Mn_2O_3 [22].

SCAN+U correctly moves predicted band gaps closer to experimental values by predicting semiconducting behavior instead of metallic behavior in Ce_2O_3, Fe_3O_4, and α-Mn_2O_3.

Interestingly, Gautam *et. al.* noticed that lower *U* values are required in SCAN compared to PBE which they attributed to reduced self-interaction error in SCAN.

Others have uncovered issues in the over-estimation of magnetic energies with SCAN. Fu and Singh [15] found that SCAN exaggerates the stability of the Fe BCC phase by over 0.593 eV/atom and the magnetic moment by 2.63 μB/atom. For elemental V, Co, Ni, and Pd, SCAN also over-estimates the magnetic energies and predicts infinite susceptibility for V; therefore, it was concluded that PBE was the more accurate functional for those metallic systems. Additionally, Isaacs *et al* noticed in intermetallic compounds that SCAN performs moderately worse than PBE with a 20% higher error in formation energy prediction.

A well-regarded functional for the treatment of bulk solids is the PBEsol functional [61], which becomes exact in the limit of solids with slowly varying densities. Hinuma *et al* [38] compared the performance of seven functionals (PBE, PBE+D3, PBE(+U), PBE+D3(+U), PBEsol, PBEsol+U, SCAN) in calculating formation enthalpies, phonon free energies, and lattice parameters of 64 bulk and 25 low-dimensional solids. It was found that PBEsol, SCAN, and PBE+D3 performs the best, even among the low-dimensional materials despite the lack of explicit vdW interactions in PBEsol and SCAN. Mis-prediction of ground states was not discussed in this work.

Therefore, we also compare the accuracy of PBEsol for predicting the ground state in a subset of 45 binary chemistries with that of the other functionals. The comparison of the five functionals for ground state structure prediction is described in Figure S2. The results are given as function of an energy window, which is the absolute energy difference between the experimentally-determined ground state and the DFT-calculated ground state. This energy window gives an additional metric for analyzing relative energy errors: the greater the energy

window necessary to reduce to a zero mis-prediction rate, the greater the magnitude of functional error in ground state structure prediction. Figure S3 indicates that the PBEsol functional does not approach the same level of structure prediction accuracy as SCAN but is, at least, more accurate than the two other GGA variants (PBE and PBE+D3). Although PBEsol does not explicitly treat vdW interactions, the non-locality, or s dependence in the exchange is actually less pronounced in PBEsol than in PBE, leading to a behavior that is more similar to LDSA. Therefore, lattice constants are not as over-estimated in PBEsol [61]. We also plot the exchange enhancement factor of PBEsol in Figure S3 alongside PBE and SCAN, and notice there is no explicit vdW interactions as there is a lack of an inflection point. Therefore, for binary ionic solids, PBEsol is not expected to reproduce the results given by SCAN.

In our study we include two variants of vdW approximations: semi-empirical PBE+D3 and the density functional approximation SCAN+rVV10. However, there are other vdW methods, such as the Fractional Ionic Approximation (FIA) [54], Tkatchenko-Scheffler (TS) [55], self-consistent screened TS [56], exchange-hole-based correction [57], and others [58] which were not tested.

We do not dismiss the possibility that another GGA-vdW method may yield more accurate statistics than PBE+D3. Certainly, for 11 layered materials, FIA benchmarked against 10 other vdW methods [53] (including SCAN+rVV10 and PBE+D3) gave better energetic and geometric properties than PBE+D3 and at reduced computational cost compared to SCAN+rVV10. It is possible that in some of the layered systems studied in this work, the ground state prediction accuracy within FIA may be more accurate.

V. Conclusion

Based on a test of 138 main group compounds where self-interaction error is not prominent, we extract systematic errors in both PBE and PBE+D3 which lead to unphysical trends in structure selection. For PBE, lack of vdW interactions in the exchange energy results in a preference for cation under-coordination. In PBE+D3, the attractive semi-empirical vdW correction consistently stabilizes closer-packed anions but does not reproduce known chemical stability rules. We argue that the origin of the increased structure selection accuracy in SCAN is the chemically-sensitive, experimentally-consistent representation of medium-ranged vdW attraction. Given the ability of this functional to capture structural stabilities across a wide range of chemistries without demonstrating systematic preference for certain local environments, we recommend SCAN as the functional of choice for evaluating polymorphic stabilities in bulk main group solids.

References

[1] P. Hohenberg and W. Kohn, Physical Review **136**, 864 (1964).

[2] W. Kohn and L. J. Sham, Physical Review **140**, 1133 (1965).

[3] A. Jain, S. P. Ong, G. Hautier, W. Chen, W. D. Richards, S. Dacek, S. Cholia, D. Gunter, D. Skinner, G. Ceder, and K. A. Persson, APL Materials **1**, 011002 (2013).

[4] D. A. Kitchaev and G. Ceder, Nat. Commun. **7**, 13799. (2016).

[5] M. E. Casida, C. Jamorski, K. C. Casida, and D. R. Salahub, J. Chem. Phys **108**, 4439 (1998).

[6] C. Stampfl, W. Mannstadt, R. Asahi, and A. J. Freeman, Phys. Rev. B **63**, 155106 (2001).

[7] C. Stampfl and C. G. Van de Walle, Phys. Rev. B **59**, 5521 (1999)

[8] J. K. Labanowski, J. W. Andzelm, Springer, New York (1991).

[9] R. J. Meier, Comput. Mater. Sci. **27** 219-223 (2003).

[10] J. P. Perdew, K. Burke, M. Ernzerhof, Phys. Rev. Lett. **77**, 3865 (1996).

[11] A. D. Becke, Phys. Rev. A **33**, 2786 (1986).

[12] A. D. Becke, ACS Symp. Ser. **394**, 165 (1989).

[13] J. Sun, B. Xiao, Y. Fang, R. Haunschild, P. Hao, A. Ruzsinszky, G. I. Csonka, G. E. Scuseria, and J. P. Perdew, Phys. Rev. Lett. **111**, 106401 (2013).

[14] J. Sun, A. Ruzsinszky, J. P. Perdew, Phys. Rev. Lett. **115**, 036402 (2015).

[15] Y. Fu, D. J. Singh, Phys. Rev. Lett. **121**, 207201 (2018).

[16] G. X. Zhang, A. M. Reilly, A. Tkatchenko, M. Scheffler, New J. Phys. **20**, 063020 (2018).

[17] C. J. Bartel, A. W. Weimer, S. Lany, C. B. Musgrave, A. M. Holder, npj Comput. Mater. **5**, 4 (2019).

[18] A. Chakraborty, M. Dixit, D. Aurbach, D. T. Major, npj Comput. Mater. **4**, 60 (2018).

[19] E. B. Isaacs, C. Wolverton, Phys. Rev. Mater. **2**, 063801 (2018).

[20] D. A. Kitchaev, H. Peng, Y. Liu, J. Sun, J. P. Perdew, G. Ceder, Phys. Rev. B **93**, 045132 (2016).

[21] M. Y. Zhang, Z. H. Cui, H. Jiang, J. Mater. Chem. A **6**, 6606-6616 (2018).

[22] G. S. Gautam, E. A. Carter Phys. Rev. Mater. **2**, 095401 (2018).

[23] Y. Zhang, J. W. Furness, B. Xiao, J. Sun, J. Chem. Phys. **150**, 014105 (2019).

[24] Y. Zhang, D. A. Kitchaev, J. Yang, T. Chen, S. T. Dacek, R. A. Sarmiento-Pérez, M. A. L. Marques, H. Peng, G. Ceder, J. P. Perdew, J. Sun, npj Comput. Mater. **4**, 9 (2018).

[25] A. Belsky, M. Hellenbrandt, V. L. Karen, P. Luksch. Acta Crystallogr. Sec. B Struct. Sci **58**, 364-369 (2002).

[26] G. Hautier, C. Fischer, V. Ehrlacher, A. Jain, G. Ceder, Inorg. Chem. **50**, 2 (2011).

[27]   S. P. Ong, W. D. Richards, A. Jain, G. Hautier, M. Kocher, S. Cholia, D. Gunter, V. L. Chevrier, K. A. Persson, G. Ceder, Comput. Mater. Sci. **68**, 314-319. (2013)

[28]   G. Kresse, J. Furthmüller, Phys. Rev. B **54**, 11169 (1996).

[29]   G. Kresse, J. Furthmüller, Comput. Mater. Sci. **6**, 15-50 (1996)

[30]   J. P. Remeika and M. Marezio, J. Am. Chem. Soc. 8, 87 (1966).

[31]   S. Geller, J. Chem. Phys. **33**, 676, 1960.

[32]   B. J. Kennedy, C. J. Howard, Phys. Rev. B, **70**, 144102 (2004).

[33]   A.A. Bolzan, C. Fong, B.J. Kennedy, and C.J. Howard, Acta Crystallogr., Sect. B: Struct. Sci. B53, 373 (1997).

[34]   G. Liu, H. A. Eick, Journal of the Less-Common Metals, **156**, 237-245 (1989).

[35]   Unruh, H. G., Mühlenberg, D. and Hahn, Ch., Z. Phys. BCond. Matter, 1992, 86, 133

[36]   J-M Léger, J. Haines, C. Danneels, J. Phys. Chem Solids, **8**, 1199-1204 (1998).

[37]   C. J. Howard, B. J. Kennedy, C. Curfs, Phys. Rev. B **72**, 214114 (2005).

[38]   Y. Hinuma, H. Hayashi, Y. Kumagai, I. Tanaka, F. Oba, Phys. Rev. B **96**, 9 094102 (2017).

[39]   C. Shahi, J. Sun, J. P. Perdew, Phys. Rev. B **97**, 9, 094111 (2018).

[40]   N. Sengupta, J. E. Bates, A. Ruzsinszky, Phys. Rev. B **97**, 235136 (2018).

[41]   L. Pauling, J. Am. Chem. Soc. **69**, 542-553 (1947).

[42]   L. Wang, T. Maxisch, G. Ceder, Phys. Rev. B **73**, 195107 (2006).

[43]   J. P. Perdew, A. Ruzsinszky, J. Tao, V. N. Staroverov, G. E. Scuseria, J. Chem. Phys. **123**, 062201 (2005).

[44]   J. P. Perdew, A. Ruzsinzsky, J. Sun, K. Burke**,** J. Chem. Phys. **140,** 18A533 (2014).

[45]   A. S. Rosen, J. M. Notestein, R. Q. Snurr, J. Comput. Chem, **9999**, 1-14 (2019).

[46]   Sanvito S., Žic M., Nelson J., Archer T., Oses C., Curtarolo S. Handbook of Materials Modeling. Springer, Cham. (2018).

[47]   A. R. Natarajan, A. Van der Ven, npj Computational Materials, **4**, 56 (2018).

[48]   H. Peng, Z. H. Yang, J. P. Perdew, J. Sun, Phys. Rev. X, **6**, 041005 (2016).

[49]   Y. Zhao, D. G. Truhlar, J. Chem. Phys. **128**, 184109 (2008).

[50]   P. Haas, F. Tran, P. Blaha, Phys. Rev. B., **79**, 085104 (2009).

[51]   E. H. Lieb and S. Oxford, Int. J. Quantum Chem. **19**, 427 (1981).

[52]   S. Grimme, J. Antony, S. Ehrlich, H. Krieg, J. Chem. Phys. **132**, 154104 (2010).

[53]   S. A. Tawfik, T. Gould, C. Stampfl, M. J. Ford, Phys. Rev. Mater. **2**, 034005 (2018).

[54]   T. Gould, S. Lebègue, J. G. Ángyán, and T. Bucko, J. Chem. Theor. Comput. **12**, 5920 (2016).

[55]   A. Tkatchenko and M. Scheffler, Phys. Rev. Lett. 102, 073005 (2009).

[56]   A. Tkatchenko, R. A. DiStasio, R. Car, and M. Scheffler, Phys. Rev. Lett. **108**, 236402 (2012).

[57]   S. N. Steinmann and C. Corminboeuf, J. Chem. Phys. **134**, 044117 (2011).

[58]   J. Harl, L. Schimka, and G. Kresse, Phys. Rev. B 81, 115126 (2010)

[59]   Supplemental Information of this paper

[60]   K. R. Tsai, P. M. Harris, E. N. Lassettre, J. Phys. Chem. **60**, 338-344 (1956).

[61]   J. P. Perdew, A. Ruzsinszky, G. I. Csonka, O. A. Vydrov, G. E. Scuseria, L. A. Constantin, X. Zhou, and K. Burke, Phys. Rev. Lett., **102**, 039902 (2009).

[62]   W. Sun, S. T. Dacek, S. P. Ong, G. Hautier, A. Jain, W. D. Richards, A. C. Gamst, K. A. Persson, G. Ceder, Science Advances, **2**, 11, (2016).

[63]   K. R. Tsai, P. M. Harris, E. N. Lassettre, J. Phys. Chem., **60**, 345 (1956).

[64]   P. Haas, F. Tran, P. Blaha, Phys. Rev. B., **79**, 085104 (2009).

[65]   A. B. Rahane, M. D. Deshpande, J. Phys. Chem. C. **116**, 2691-2701 (2012).

[66]   K. A. Mengle, G. Shi, D. Bayerl, E. Kioupakis, **109**, 212104 (2016).

[67]   H. J. von Bardeleben, S. Zhou, U. Gerstmann, D. Skachkov, W. R. L. Lambrecht, Q. D. Ho, P. Deák, APL Materials, **7**, 022521 (2019).

[68]   R. A. Howie, W. Moser, I. C. Trevena, Acta Crys. **28**, 2965, (1972).

[69]   S. A. Hodorowicz, H. A. Eick, Journal of Solid State Chemistry **46**, 313-320 (1983).

[70]   M Blackman, I H Khan, Proc. Phys. Soc. **77**, 471, (1961).

[71]   A. V. Churilov, G. Ciampi, H. Kim, W. M. Higgins, L. J. Cirignano, F. Olschner, V. Biteman, M. Mincello, K. S. Shah. J. Cryst. Growth, 312, 1221-1227 (2010).

[72]   G. A. Samara, L. C. Walters, D. A. Northrop, Journal of Physics and Chemistry of Solids, 28, 10, (1967).

[73]   K. Momma and F. Izumi, J. Appl. Crystallogr., **44**, 1272-1276 (2011).

Acknowledgements